Chapter 2
The CMS Experiment at the LHC

Since the very first measurements with α particles performed by H. Geiger, E. Marsden and E. Rutherford [1], scattering experiments have become one of the most important tools in experimental particle physics. Increasing collision energies allow to resolve smaller and smaller structures, and to probe the fundamental constituents of matter and their interactions.

Modern particle accelerators provide the possibility to produce collisions in a controlled and well-understood environment. Beams of electrons, protons or nuclei are accelerated to high energies and brought to collision by intersecting them at one or several intraction points. Large and complex particle detector systems are built around these intraction points in order to measure the properties of the emerging collision products.

The LHC marks a milestone in the development of particle accelerators. It provides particle collisions at unprecedented energies and with a twenty-fold increase in instantaneous luminosity compared to its predecessor Tevatron. This chapter briefly describes both the LHC accelerator and the CMS experiment. Section 2.1 covers some basic aspects of the LHC and introduces the concept of luminosity, while Sect. 2.2 provides an overview of the CMS experiment and its subdetector systems. Finally, Sect. 2.3 gives a brief outlook on forthcoming upgrades of the CMS experiment.

2.1 The Large Hadron Collider

The Large Hadron Collider (LHC) is currently the largest particle accelerator world wide with a circumference of 27 km and a design center-of-mass energy of 14 TeV. It is located at the European Organization for Nuclear Research (CERN) in Geneva and resides 100 m below ground in the tunnel originally excavated for the Large

S. Spannagel, *CMS Pixel Detector Upgrade and Top Quark Pole Mass Determination*, Springer Theses, DOI 10.1007/978-3-319-58880-3_2

Electron-Positron (LEP) [2]. The LHC operates in either proton-proton, proton-nuclei or nuclei-nuclei collision mode, of which only the proton mode is discussed here.

The protons are generated by ionizing ultrapure hydrogen. Before being injected into the LHC, the protons are accelerated to the injection energy of 450 GeV by a series of pre-accelerators, namely a linear accelerator, the Proton Synchrotron (PS), and the Super Proton Synchrotron (SPS). This pre-accelerator complex is also used for other experiments such as NA62 at the SPS [3], irradiation of detector samples and material at the PS, or test beams at the SPS-fed Experimental Hall North beamlines.

In the LHC the two counter-rotating proton beams circulate in two evacuated beam pipes. The beams are kept on orbit and in focus by the magnetic field of superconducting dipole and quadrupole magnets, and are accelerated by radio frequency cavities. All magnets and cavities are cooled down to 1.9 K by liquid helium to maintain the superconducting regime. Additional magnets are used for focusing of the beams at the interaction point (IP) of the respective experiment.

At nominal beam configuration, the LHC contains 2808 bunches with a bunch spacing of 25 ns. After initial problems with the quench protection of the dipole magnets, the LHC operated at $\sqrt{s} = 7\,\text{TeV}$ from 2010 to 2011, and at 8 TeV in 2012. The center-of-mass energy of $\sqrt{s} = 13\,\text{TeV}$ has only been reached after the Long Shutdown 1 (LS1) conducted from 2013 to 2015. First papers using data recorded at $\sqrt{s} = 13\,\text{TeV}$ have already been published [4].

More detailed information on the LHC machine can be found elsewhere [5, 6].

2.1.1 Luminosity and Event Rate

The rate dN/dt of events of a given process depends on the cross section σ of the process under investigation and on the instantaneous luminosity $\mathcal{L}$, viz.

$$\frac{dN}{dt} = \sigma \cdot \mathcal{L}. \tag{2.1}$$

The instantaneous luminosity $\mathcal{L}$ is a function of beam parameters and defined as

$$\mathcal{L} = \frac{N_b N_p^2 f}{A}, \tag{2.2}$$

where N_b denotes the number of bunches in the ring, N_p the number of protons per bunch, and $f \approx 11\,\text{kHz}$ is the revolution frequency around the ring. Parameter A is the effective cross section of the beam and depends on the beam focus as well as the beam crossing angle and the size of the bunches.

The LHC has been designed to deliver an instantaneous luminosity of $\mathcal{L} = 1 \times 10^{34}\,\text{cm}^{-2}\,\text{s}^{-1}$ with a nominal filling of $N_p = 1.15 \times 10^{11}$ protons per bunch. In order to limit beam-beam interactions, the LHC has been operating with a bunch spacing of 50 ns and thus a reduced number of 1374 bunches in the ring until summer 2015. The proton intensity per bunch had been increased [7] to reach the intended instantaneous luminosity. However, this leads to a higher pile-up (cf. Sect. 1.2.3) and is a challenge for the experiments due to higher occupancy of the detectors.

To obtain the total number of events recorded for a given process, Eq. 2.1 has to be integrated over time. The integrated luminosity $\int \mathcal{L}dt$ is usually given in units of inverse femto barn fb^{-1}, where $1\,\text{b} = 1 \times 10^{-24}\,\text{cm}^2$.

In 2012, a maximum instantaneous luminosity of $7.7 \times 10^{33}\text{cm}^{-2}\text{s}^{-1}$ was reached and a total integrated luminosity of $\int \mathcal{L}dt = 21.8\,\text{fb}^{-1}$ has been recorded by the CMS experiment [8] as depicted in Fig. 2.1. Data corresponding to an integrated luminosity of $19.7\,\text{fb}^{-1}$ have been validated and released for physics analysis as shown in Fig. 2.1b.

The instantaneous luminosity can be obtained from the inverse of Eq. 2.1. By measuring the event rate of a process with precisely known cross section, the luminosity can be calculated. In the CMS experiment the current method for online luminosity measurement is the so-called *zero-counting* method using information from the hadronic calorimeter [10]. For offline luminosity determination in recorded data, several different methods are available [11]. The luminosity presented in Fig. 2.1 is obtained using the *pixel-cluster-counting* method which counts the number of clusters in the pixel system per bunch crossing [12].

The absolute luminosity calibration is performed with Van-der-Meer separation scans [13] in which the event rates of the online luminosity method is measured as a function of transverse beam separation. This allows to determine the effective beam profile and to calculate the absolute luminosity according to Eq. 2.2.

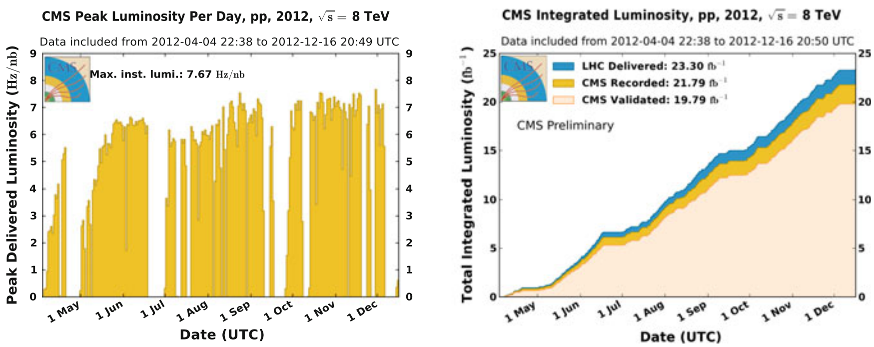

(a) Instantaneous luminosity for the 2012 LHC running period. From [8].

(b) Integrated luminosity delivered, recorded, and validated (beige). From [9].

Fig. 2.1 Evolution of the instantaneous (**a**) and integrated (**b**) luminosity. *Blue* denotes the luminosity delivered by the LHC while *orange* marks the luminosity recorded by the CMS experiment (colour figure online)

2.1.2 Experiments

The LHC ring supplies four main experiments as well as a set of smaller detectors with particle collisions.

The experiments A Toroidal LHC ApparatuS (ATLAS) [14] and Compact Muon Solenoid (CMS) [15] are the two large general purpose detectors at the LHC. The detectors are not tailored to one specific measurement, but are designed to be able to cover a broad range of physics. Their main objectives are precision measurements of the SM, discovery and exploration of the mechanism of EWSB, and to shed light on physics beyond the SM and possible explanatory theories as discussed in Sect. 1.1.4.

The A Large Ion Collider Experiment [16] is dedicated to heavy ion physics with the principal goal being the investigation of quark-gluon plasma. The Large Hadron Collider beauty (LHCb) [17] experiment is specialized in physics involving hadrons with b-quark content.

The two smaller experiments LHCf [18] and TOTEM [19] measure the total inelastic cross section of proton-proton collisions. Both are so-called *forward experiments* and are located in vicinity to the ATLAS and CMS experiments, respectively. The Monopole and Exotics Detector At the LHC MoEDAL [20] has been installed in the vicinity of the LHCb IP during the LS1 and will commence its search for magnetic monopoles and other exotica soon.

2.2 The Compact Muon Solenoid

The Compact Muon Solenoid (CMS) experiment [15, 21] is one of the two general purpose detectors at the LHC and located at the interaction points 5 near the french village Cessy. With a length of 21.6 m, a diameter of 14.6 m and a gross weight of 14000 t it is one of the largest and most complex particle detectors built to date.

Its design is driven by the challenges of high energy physics at hadron colliders. Many interesting physics channels exhibit only a small cross section, while QCD jet production dominates the background contributions. Especially the precise reconstruction of lepton signatures is vital for the detection of many rare processes, and an optimal efficiency at high rejection power of background events is required. The CMS detector is designed following the concept of excellent muon and electron identification and momentum resolution. This is rendered possible by the high granularity of the electromagnetic calorimeter and the extensive muon tracking systems described in Sects. 2.2.2 and 2.2.4, respectively.

For an efficient identification of heavy flavor quarks and τ lepton decays the precise measurement of secondary vertices and impact parameters is essential. The 3.8 T superconducting solenoid described in Sect. 2.2.3 provides the bending power for a good p_T discrimination of traversing particles by the all-silicon pixel and strip tracking detectors. These inner tracking detectors are introduced in Sect. 2.2.1 and allow for the precise determination of particle trajectories and vertices.

CMS employs a right-handed coordinate system to describe positions in the experiment [21]. The z-axis is defined along the LHC proton beam, while the x-axis points towards the center of the LHC ring. The equivalent polar coordinates are defined as follows. The radial distance from the beam pipe is denoted as r, the polar angle θ is measured with respect to the z-axis, and the azimuthal angle ϕ is measured against the x-axis. Usually the pseudorapidity η is favored over the polar angle and is defined as

$$\eta = -\ln \tan \theta/2. \tag{2.3}$$

Momentum and energy transverse to the beam are denominated as p_T and E_T, respectively. Missing energy in the transverse x-y-plane is denoted as E_T^{miss}.

2.2.1 Tracking Detectors

CMS features an all-silicon tracking system with a total active area of about 200 m^2 covering the solid angle up to pseudorapidities of $|\eta| < 2.5$. It consists of a high-granularity pixel detector close to the interaction region and a silicon strip tracker which covers radii from 0.2 to 1.2 m as depicted in Fig. 2.2.

The demands on the tracking system are high: At LHC design luminosity more than 1000 charged particles emerge from the interaction region every bunch crossing, passing through the tracking detectors and leaving hit information. This information needs to be buffered until the event has been validated by a trigger signal and the full event information is retrieved from all detectors (cf. Sect. 2.2.5). At the same time the overall material budget has to be minimized in order not to deteriorate both

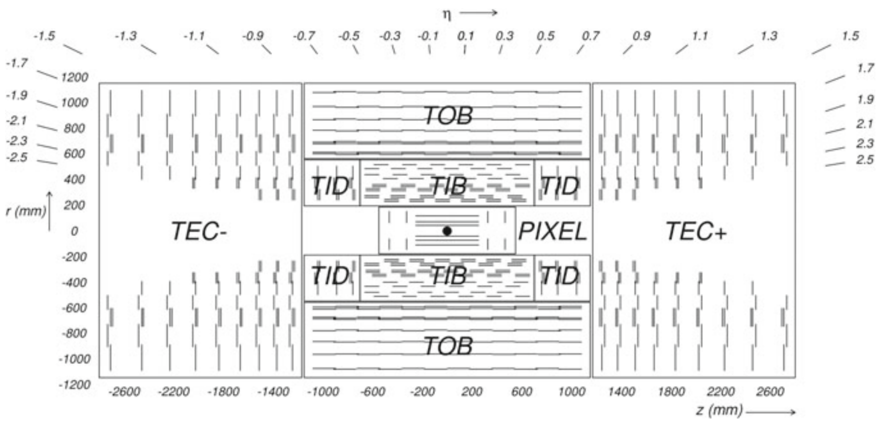

Fig. 2.2 Geometry of the CMS inner tracking system. Shown is the rz view of the detector with the positions of the subdetectors and their modules. *Double lines* indicate back-to-back mounted modules for stereo angle interpolation, the nominal IP is marked with a *black dot*. From [15]

the momentum measurements via multiple Coulomb scattering and the calorimetric energy measurement by early energy loss. Moreover, the large flux of ionizing particles near the intraction point requires radiation hard tracking detectors and front-end electronics, especially since these detectors are operated for almost a decade without the possibility of maintenance or repair.

Since LS1 the tracking detectors are operated at temperatures below $-15\,^{\circ}\mathrm{C}$ to mitigate effects from radiation damage and reduce the leakage current through the sensor (cf. Sect. 3.1).

The Silicon Pixel Detector

The CMS Pixel Detector consists of three concentric barrel layers at radii of 4.4, 7.3, and 10.2 cm as well as two endcap discs on each side at distances of $z = \pm 34.5$ cm and ± 46.5 cm from the nominal interaction point. The pixel detector covers a pseudo-rapidity range up to $|\eta| \leq 2.2$ with three hits, and $2.2 < |\eta| < 2.5$ with two hits per trajectory with single hit detection efficiencies above 99% [22].

The detector consists of 1440 modules comprising the segmented silicon sensor with a pixel pitch of $100\,\mu\mathrm{m} \times 150\,\mu\mathrm{m}$ as well as the front-end electronics. In total, the detector has about 66 million readout channels which are operated in zero-suppression mode. Only pixels with a charge above an individually configurable threshold contribute to the event data. The pulse height information of every pixel hit as well as the pixel address are transmitted as analog signal and sampled by analog-digital converters (ADCs) in the front end drivers (FEDs) of the CMS data acqisition (DAQ) system.

The geometry of the pixel detector and the pixel sensor cells has been carefully chosen to yield optimal spatial resolution. While the barrel modules are mounted with the sensor surface parallel to the magnetic field of the solenoid, the forward detector modules in the endcaps are tilted by 20°. By this, the charge carriers produced by a charged particle traversing the detector are distributed over several pixels, either by the Lorentz drift or by the geometrical arrangement. This permits interpolation of the charges to calculate a more precise track impact point (cf. Sect. 3.3). The intrinsic spatial resolution of the detector has been determined to be $10\,\mu\mathrm{m}$ in the $r\phi$ direction, and 20–45 μm along the z axis, depending on the incidence angle of the particle track [22].

The pixel detector will be replaced by a new detector in the extended year-end technical stop of the LHC 2016/2017. This so-called phase I Pixel Detector is described in detail in Chap. 4.

The Silicon Strip Tracker

Around the pixel detector, the silicon strip tracker of CMS is located. Instead of segmenting the silicon sensor in two dimensions, the strip sensors feature implants which are divided into long strips. This allows to reduce both the very high manufacturing cost of a pixel detector caused by the complicated front-end electronics and bump bonding process, and the granularity of the detector while covering large areas.

The layout of the CMS tracker can be inferred from Fig. 2.2. The Tracker inner barrel (TIB) and Tracker inner disks (TIDs) are located around the pixel detector in the center, while the Tracker outer barrel (TOB) and Tracker endcaps (TECs) form the outermost part of the tracker. Additional thermal shielding and air-tight sealing shields the tracker volume from the surrounding detector and allows flushing with dry air. This is of importance since the tracker is operated at temperatures of around -15° and the humidity has to be controlled in order to avoid condensation.

In order to provide a measurement for the second local coordinate, some of the detector modules consist of two strip sensors which are mounted back-to-back and rotated by a small stereo angle with respect to each other. Correlating the responses of the two sensors in the offline analysis allows to reconstruct the missing coordinate. However, this concept only performs well at low occupancy since the signal will otherwise be dominated by matching ambiguities.

Tracking

CMS employs a combinatorial Kalman filter (CKF) for tracking [23, 24]. The CKF is a recursive procedure which estimates the track parameters starting from an initial trajectory and updates the estimators with every successive hit added to the trajectory. Several methods are being used within CMS with the *inside-out* approach being the most prevalent one [25].

The track fitting is performed in three consecutive stages. Initial trajectory candidates, so-called *seeds*, are constructed from pixel detector information including constraints on the position of the beam spot and on a minimal transverse momentum p_T. This approach makes use of the high precision measurement of the pixel detector with its fine granularity and the very clean, low-noise signal.

The trajectories built from the initial seeds are then propagated from layer to layer to the outside, always accounting for multiple scattering and energy loss. The track parameters and uncertainties are updated on every layer, and new trajectories are created for every compatible hit. The total number of track candidates is limited by a maximum global X^2 requirement of the track fit and by the number of missing hits for the complete trajectory. Ambiguities are solved by selecting the best trajectories based on the overall track fit quality and the number of shared hits.

After all information has been added to the track candidates, the final track fit is performed. The track resolution already reaches an asymptotic value after the first five hits have been added to the candidate. This enables the high level tigger (HLT) (cf. Sect. 2.2.5) to use tracking information, and allows to interrupt the tracking procedure as soon as enough information is acquired. These tracks are used for online vertex reconstruction and b-tagging [23].

Precise and stable tracking is especially important for the partical flow (PF) algorithm described in Sect. 12.2, which relies on tracking every single charged particle and assigning it to a calorimeter cluster.

2.2.2 Calorimeters

The task of measuring the particle energy is accomplished by the calorimeter detectors. Calorimeters are usually made of high-density materials in which the particles initialize showers as described in Sect. 1.3.2. In order to gain information about both the energy and the direction of the particles, calorimeter detectors are segmented. This allows to distinguish multiple particles or jets and enables matching with the tracks recorded by the tracker system (cf. Sect. 12.2).

Electromagnetic Calorimeter

The CMS Electromagnetic (ECAL) measures the energy of particles which primarily interact via the electromagnetic force. It is a hermetic detector covering the solid angle up to pseudorapidities of $|\eta| < 3$. The ECAL is divided into the barrel calorimeter (EB), the endcap calorimeter (EE), and is completed by the additional preshower calorimeter (ES) as shown in Fig. 2.3.

The detector consists of scintillator crystals made of lead tungstate ($PbWO_4$). These crystals provide both a very fast response time [26] and a high radiation tolerance, both being crucial parameters for the ECAL. The high density of $8.3\ \mathrm{g/cm^3}$ allows for the construction of a relatively compact calorimeter while still containing most of the showers. With a crystal length of 23 cm in the barrel region, and 22 cm in the endcaps, the ECAL provides $25.8\,X_0 (22\,X_0)$ of showering material in the barrel (endcap) detector. The ES preshower adds additional $3\,X_0$ of lead absorbers with silicon strip sensors in the pseudorapidity range $1.65 < |\eta| < 2.6$, before the EE detector. The light output of the scintillator crystals varies strongly with temperature and makes temperature stabilization of the ECAL detector a necessity.

The fine granularity of the detector using crystal faces with a size of $22 \times 22\ \mathrm{mm}^2$ in the barrel detector and $28.6 \times 28.6\ \mathrm{mm}^2$ in the endcaps provides good angular

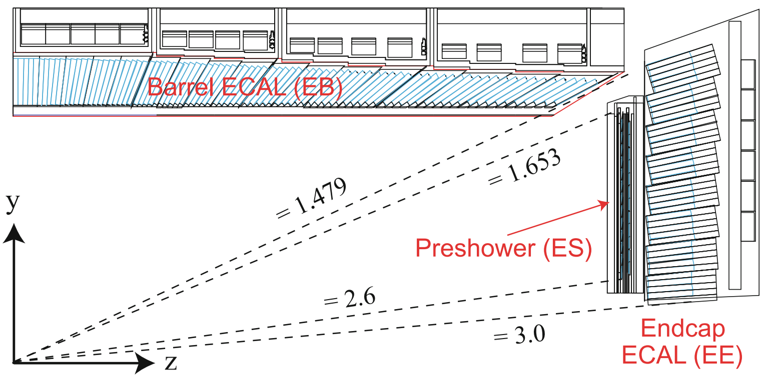

Fig. 2.3 Geometry of the CMS electromagnetic calorimeter. Shown is one transverse section through the ECAL indicating the positions of the EB, the EE and the ES detectors. From [21]

resolution and allows for precise matching with the tracking information using the PF algorithm (cf. Sect. 12.2).

The scintillation light from every crystal is detected by avalanche photo diode and vacuum phototriode in the EB and the EE detectors, respectively. Both devices have been extensively characterized in magnetic fields and under heavy irradiation to ensure stable operation for more than ten years.

Hadronic Calorimeter

The energy of hadrons is measured by the CMS Hadron Calorimeter (HCAL), a sampling calorimeter composed of alternating layers of massive absorbing brass plates and plastic scintillator tiles. Just like the other subdetector systems, it is divided into a barrel part comprising the barrel (HB) and tail-catching outer calorimeter (HO) up to $|\eta| < 1.3$, and endcap detectors. The endcaps include the endcap calorimeter (HE) for the pseudorapidity range $1.3 < |\eta| < 3$ and the additional forward calorimeter(HF) extending the HCAL acceptance up to $|\eta| < 5.2$ for hermetic coverage of the solid angle.

The barrel detector separation into HB and HO arises from the limited space available to the barrel detector. The HB detector is located inside the coil of the superconducting magnet, and is supplemented by the HO located outside the solenoid coil, right before the muon chambers. The HO thus works as tail-catcher to improve the energy measurement of jets and E_T^{miss} [27, 28]. It uses the solenoid itself as absorber material. Combining HB and (HO), the barrel HCAL provides material to contain showers up to 11.8 interaction lengths λ_{int}.

The scintillation light collected from the scintillator tiles is converted using wavelength shifting fibers, and measured by hyprid photodetectors (HPDs) [29] which will eventually be replaced by silicon photomultipliers (SiPMs) as detailed in Sect. 2.3. During the LS1, the HO detector has already been completely equipped with SiPMs [30]. To improve the detection of early showers developing in the material between ECAL and HCAL, the first layer of scintillating tiles are placed before the first absorber plate. The last layer of scintillator tiles is located behind the last absorber layer in order to detect late showers which are leaking out of the detector.

The HF is exposed to a high level of radiation despite its remote location at $z = \pm 11.2$ m away from the nominal interaction point and thus uses a different detection technology. Energies of around 760 GeV at center-of-mass collision energies of 14 TeV are deposited in the HF, compared to an average of 100 GeV in the rest of the HCAL, and require the use of steel absorbers with embedded quartz fibers. These fibers detect the Cherenkov light produced by charged particles in the developing showers and are thus mainly sensitive to the electromagnetic fraction of the hadronic shower (cf. Sect. 1.3.2).

For jets with an energy of 50 GeV the relative energy resolution of the combined ECAL and HCAL detector systems is about 15% as obtained from test beam data. This can be greatly reduced by applying the PF algorithm described in Sect. 12.2. A detailed introduction to hadron calorimeters as well as a comparison of the hadron calorimeter performance of the ATLAS and CMS experiments can be found in [31].

2.2.3 The Solenoid

The design of the CMS experiment is centered around its strong superconducting solenoid magnet, which provides a 3.8 T magnetic field. This allows for a precise measurement of the particle momenta owing to the large bending power. The 13 m long coil has an inner diameter of 6 m which allows to house the tracking detectors and to also comprise the calorimetric systems. This improves the energy resolution significantly since the particles do not lose energy by crossing the magnet coil prior to being measured.

The stored energy at full magnetic field is about 2.6 GJ, with the magnetic flux returned through an iron return yoke. The return yoke also hosts the muon systems, and the 2 T magnetic return field allows for precise muon momentum determination.

2.2.4 Muon Systems

Muons at moderate energies can be considered minimum ionizing particles (MIPs) and traverse both the tracker and the calorimeters with minimal energy loss. They can thus be efficiently identified by a dedicated muon detector system outside the calorimeters which provides additional information for tracking. Due to the unique characteristics, the muon signal often has a superior signal-to-noise ratio and is heavily used in both trigger and physics analyses.

The muon systems form the outermost part of the CMS detector and are integrated into the magnet return yoke surrounding the solenoid. Gaseous detector chambers have been chosen as the technology for the muon system, providing cost efficient coverage of almost the full solid angle.

Three different types of detectors are employed, depending on their mounting position in the experiment. So-called drift tubes (DTs) are used in the barrel region of the detector, where the magnetic field is homogeneous and both the muon rate and the neutron induced backgrounds are comparatively low. The four layers of (DT) modules cover a pseudorapidity range up to $|\eta| < 1.2$. Each DT station hosts 12 individual, gas-filled tubes with a diameter of 4 cm and a center electrode. Most of the tubes run along the z axis providing measurements in $r\phi$, whereas the first three layers also feature tubes for z measurement.

The endcap regions covering $0.9 < |\eta| < 2.4$ are subject to a much higher muon flux while the magnetic field is stronger and less homogeneous. Therefore, cathode strip chambers (CSCs) are deployed which feature a faster response time, higher granularity, and better radiation hardness. The CSCs are trapezoidal multi-wire proportional chamber which provide 2D position measurements with the cathode strips running radially from the beampipe.

Resistive plate chambers (RPCs) in both the barrel and the endcap regions provide precise timing information of the order of 1 ns at the cost of a coarser position resolution and are mainly used for bunch crossing assignment and in the trigger system.

They consist of two high-resistivity plastic plates with readout strips, separated by a gas-filled volume. The RPCs are operated in avalanche mode.

During LS1, a fourth endcap muon station has been installed, and the readout electronics of the (CSCs) and (DTs) have been improved.

2.2.5 The Trigger and Data Acquisition System

With the LHC delivering proton-proton collisions at a rate of 40 MHz, the data produced by the CMS experiment are orders of magnitudes too large to be stored. The typical size of one event recorded by the CMS detector is about 1 MB, and it would be technically impossible to stream about 40 TBs^{-1} to disk. However, even if possible, the added scientific value would be questionable since most of the events only contain low-energy glancing collisions rather than inelastic hard scattering processes.

The required reduction of the event rate is achieved by the so-called trigger system. The task of the trigger is the selection of potentially interesting events and the reduction of the rate to a manageable value of a few hundred Hz.

While most high energy physics experiments use three trigger levels, the CMS trigger system implements a two-stage rate reduction which provides additional flexibility. The first stage is the Level 1 Trigger (L1) [32] which is fully implemented in hardware using Field Programmable Gate Arrays (FPGAs) and Application Specific Integrated Circuites (ASICs). It reduces the initial rate to around 100 kHz with a maximum latency of 3.4 μs, limited by the tracker system readout. During this latency all data are buffered in pipelines in the detector front-end electronics. Because of this time constraint, only data from the calorimeters and the muon systems are processed and contribute to the trigger decision. First, simplified local reconstruction algorithms are executed in the subdetector systems, and trigger primitives are generated and subsequently merged into the L1 global trigger decision. Only after a L1 acceptance signal has been issued, all subdetector systems send their buffered data to the DAQ system.

The data are then collected and synchronized by the event builder and sent to the next stage of the triggering system, the high level trigger (HLT) [33]. The HLT is software based and consists of several thousand CPUs running analysis algorithms for a full reconstruction of all events in search of interesting signatures. Time-consuming algorithms, such as tracking using the full silicon tracker information, are only applied to regions of interest since the latency of the HLT is limited to 50 ms. Events are finally stored for offline analysis if the requirements of at least one of the trigger paths are met. These trigger paths are configurable and are described in the trigger menus [34].

In case of very high rates, single trigger paths can also be prescaled to only store a fraction of the triggered events to disk. In addition, CMS also records so-called minimum bias data which are subject to only very few constraints. These data are for instance used to model the underlying event.

The final event rate which is transmitted to the CERN Tier-0 computing center and stored on tape is about 100–300 Hz.

2.3 Upgrades to the CMS Experiment

The CMS detector will undergo several major upgrades during the next decades of its operation owing to the challenges arising from higher luminosities, the performance degradation induced by damage from ionizing radiation, and to the availability of new technologies. These upgrades aim at sustaining and improving the overall performance under the increasingly demanding conditions imposed by the LHC operation. Furthermore, the maintainability of the experiment over this long period of operation has to be ensured.

The LHC schedule and the experiment upgrade plans are divided into two parts. During the Phase I until 2023 the LHC will operate at an energy of $\sqrt{s} = 13\,\text{TeV}$, and the instantaneous luminosity will be increased up to $\mathcal{L} = 2 \times 10^{34}\,\text{cm}^{-2}\text{s}^{-1}$. For this period, two long shutdowns are planned of which the first (LS1) has just been successfully completed, and improvements to the subdetector systems of CMS have been installed which allow to fully exploit the luminosity delivered by the LHC.

After 2023 a major machine upgrade will be carried out in the extended long shutdown LS3 to achieve higher instantaneous luminosities. This marks the start of the Phase II and the operation of the High-Luminosity LHC (HL-LHC). Also the CMS experiment will undergo major transformations in order to handle the higher luminosities, such as the replacement of the full inner tracking system.

2.3.1 The Phase I Upgrades

The challenges addressed by the Phase I upgrades concern both the instantaneous and the integrated luminosity experienced by the CMS experiment. With the high instantaneous luminosity delivered by the LHC, the experiment has to deal with an in-time pile-up of 60 and more, creating numerous problems for subdetectors and the L1 trigger.

Since the trigger performance would decrease at high pile-up, some parts of the trigger system such as the regional calorimeter trigger will be rebuilt using new technologies available [35]. This allows to use the full detector granularity including the additional CSC stations added during LS1 and will enable the trigger to cope with higher occupancies and more complex events. Furthermore, a new timing and trigger control system based on modern telecommunication technology will be implemented for improved performance.

Towards the end of Phase I, CMS will have collected a total integrated luminosity of about $300\,\text{fb}^{-1}$. The absorbed ionizing radiation damages the detector material and some subsystems will be subject to severe efficiency loss. Especially the pixel detector system and the HF absorb high doses.

The pixel detector will be completely replaced with a new detector featuring four barrel layers and three disks at each end. High bandwidth readout electronics will improve the efficiency at high occupancies, while relocated service electronics and a lightweight support structure will reduce the material budget in the tracking volume. A CO_2-based two-phase cooling allows for a lower operational temperature. The new pixel detector and its components are described elaborately in Chap. 4.

The HCAL upgrade plans [36] comprise new QIE10/QIE11 ADC chips as well as new control electronics to reduce single event upsets (SEUs). All HPDs in the HE and HB detector systems will be replaced with SiPMs. The HPDs faced several problems with electrical discharges, gain drifts, and increased noise levels, while the proposed SiPMs have a better quantum efficiency, higher gain, and better immunity to magnetic fields. Due to the small size of the SiPMs, the replacement also facilitates an additional depth segmentation of the detector which improves tracking of the shower development. In the HF detector, the existing photomultiplier tubes (PMTs) will be replaced with multi-anode tubes.

A more detailed description of all improvements planned and implemented for the CMS Phase I upgrades can be found in the technical proposal [37].

2.3.2 The Phase II Upgrades

The main goal of the HL-LHC operation is a recorded integrated luminosity of $3000\,\text{fb}^{-1}$ by 2035. The conditions foreseen are an average pile-up of about 140 and a leveled instantaneous luminosity of $\mathcal{L} = 5 \times 10^{34}\,\text{cm}^{-2}\text{s}^{-1}$. The main challenges for the CMS experiment are similar to those of Phase I but more severe. The detectors will experience significant radiation damage which leads to a progressive degradation of the overall detector performance. As comparison, the annual dose expected to be delivered to the detector per year at the HL-LHC is similar to the total dose received in all operations from the start of the LHC up to LS3.

The dose as well as the effect of the radiation damage vary strongly from subdetector to subdetector. The two detectors affected most are the silicon tracker and the forward calorimeters. In silicon, ionizing and non-ionizing radiation induce surface and bulk damage, leading to an increased leakage current through the sensor, trapping of charge carriers on their drift to the readout electrodes, and defects in the front-end electronics. In order to fully deplete the sensor material, the bias voltage has to be increased until it reaches an unsustainable level, while operating partial depleted sensors leads to a degradation of the signal. In the calorimeters the main problem has been identified as the transport of the scintillation light from the point of the particle interaction to the readout electronics. Especially the $PbWO_4$ crystals lose their translucence leading to a reduced signal.

The second main challenge concerns pile-up. At the nominal luminosity of the HL-LHC the pile-up is expected to be around 140 on average, but further increase of the luminosity results in higher pile-up. This causes a higher occupancy in the tracking system and will eventually lead to an increased rate of misidentified tracks. Also the identification of isolated leptons will become more challenging with more soft interactions accompanying the hard scattering process.

In order to deal with these demands and to maintain an adequate track reconstruction performance, the granularity of both the strip tracker and the pixel detector will be increased by a factor of 4. Special double-sensor modules in the strip tracker will be capable of providing p_T-discriminated track information to the L1 trigger at 40 MHz and thus reducing the data by a factor of 20. This permits powerful background rejection already at the earliest stage of event selection.

The calorimeters will be replaced by a high-granularity calorimeter with an electromagnetic and a hadronic section. The electromagnetic part uses silicon sensors as active material and provides around 25 X_0 but only about 1 λ_{int} hadronic interaction lengths. The hadronic part comprises a front section also featuring silicon sensors and provides a depth of 3.5 λ_{int}. It is followed by the backing hadron calorimeter with a design similar to the current HE calorimeter (cf. Sect. 2.2.2), providing an additional depth of approximately 10 λ_{int}.

The muon systems will be enhanced in the region $1.4 < |\eta| < 2.4$ with additional chambers in order to maintain a good L1 muon trigger acceptance. In some regions with high magnetic fields, gas electron multiplier chambers will be used.

The L1 trigger latency will be increased to 12.5 µs which is sufficient for hardware track reconstruction using new technologies such as associative memory. This implies upgrades to many of the existing readout electronics of subdetector systems. The L1 accept rate will be increased to 500 kHz at a pile-up of 140, and to 750 kHz at pile-up 200. The HLT is expected to have an output rate of up to 10 kHz.

Extensive design studies have been carried out, and detector prototypes are in production, but many projects are still in their R&D phase and changes to these proposals are to be expected. A more elaborate description of the proposed design and infrastructure for Phase II operation of the CMS experiment can be found in the technical proposal [38].

References

1. E. Rutherford, The scattering of α and β particles by matter and the structure of the atom. Philos. Mag. **21**(125), 669–688 (1911). doi:10.1080/14786440508637080
2. S. Myers, E. Picasso, The design, construction and commissioning of the CERN large electron positron collider. Contemp. Phys. **31**(6), 387–403 (1990). doi:10.1080/00107519008213789
3. NA62 Collaboration, NA62: Technical Design Document, Technical report NA62-10-07, CERN, Geneva, Dec (2010)
4. CMS Collaboration, Pseudorapidity distribution of charged hadrons in proton-proton collisions at $\sqrt{s} = 13$ TeV. Phys. Lett. B **751**, 143–163 (2015). doi:10.1016/j.physletb.2015.10.004, arXiv:1507.05915
5. L. Evans, P. Bryant, LHC machine. J. Instrum. **3**(08), S08001 (2008). doi:10.1088/1748-0221/3/08/S08001
6. O.S. Bröning et al., LHC Design Report, CERN, Geneva (2004)
7. M. Lamont, Status of the LHC. J. Phys. Conf. Ser. **455**(1), 012001 (2013). doi:10.1088/1742-6596/455/1/012001
8. CMS Collaboration, CMS Luminosity - Public Results (2012), https://twiki.cern.ch/twiki/bin/view/CMSPublic/LumiPublicResults. Accessed 09 Aug 2015

9. CMS Collaboration, Public CMS Data Quality Information (2013), https://twiki.cern.ch/twiki/bin/view/CMSPublic/DataQuality. Accessed 06 Dec 2015
10. CMS Collaboration, Measurement of CMS Luminosity, CMS Physics Analysis Summary CMS-PAS-EWK-10-004, CERN, Geneva (2010)
11. CMS Collaboration, Absolute Calibration of the Luminosity Measurement at CMS: Winter 2012 Update, CMS Physics Analysis Summary CMS-PAS-SMP-12-008, CERN, Geneva (2012)
12. CMS Collaboration, CMS Luminosity Based on Pixel Cluster Counting - Summer 2013 Update, CMS Physics Analysis Summary CMS-PAS-LUM-13-001, CERN, Geneva (2013)
13. S. van der Meer, Calibration of the effective beam height in the ISR, Technical report CERN-ISR-PO-68-31, CERN, Geneva (1968)
14. ATLAS Collaboration, The ATLAS experiment at the CERN large hadron collider. J. Instrum. **3**, S08003 (2008). doi:10.1088/1748-0221/3/08/S08003
15. CMS Collaboration, The CMS experiment at the CERN large hadron collider. J. Instrum. **3**, S08004 (2008). doi:10.1088/1748-0221/3/08/S08004
16. ALICE Collaboration, The ALICE experiment at the CERN large hadron collider. J. Instrum. **3**, S08002 (2008). doi:10.1088/1748-0221/3/08/S08002
17. LHCb Collaboration, The LHCb detector at the large hadron collider. J. Instrum. **3**, S08005 (2008). doi:10.1088/1748-0221/3/08/S08005
18. LHCf Collaboration et al., The LHCf detector at the CERN large hadron collider. J. Instrum. **3**(08), S08006 (2008). doi:10.1088/1748-0221/3/08/S08006
19. TOTEM Collaboration, The TOTEM experiment at the CERN large hadron collider. J. Instrum. **3**(08), S08007 (2008). doi:10.1088/1748-0221/3/08/S08007
20. J.L. Pinfold, The MoEDAL experiment at the LHC. EPJ Web Conf. **71**, 00111 (2014). doi:10.1051/epjconf/20147100111
21. CMS Collaboration, CMS Physics Technical Design Report Volume I: Detector Performance and Software, Technical Design Report CERN-LHCC-2006-001, CERN (2006)
22. CMS Collaboration, CMS Tracker Detector Performance Results (2012), https://twiki.cern.ch/twiki/bin/view/CMSPublic/DPGResultsTRK. Accessed 10 Aug 2015
23. CMS Collaboration, Description and performance of track and primary-vertex reconstruction with the CMS tracker. J. Instrum. **9**(10), P10009 (2014). doi:10.1088/1748-0221/9/10/P10009, arXiv:1405.6569
24. R. Frühwirth, Application of Kalman filtering to track and vertex fitting. Nucl. Instr. Methods Phys. A **262**(2–3), 444–450 (1987). doi:10.1016/0168-9002(87)90887-4
25. T. Speer et al., Track reconstruction in the CMS tracker. Nucl. Instr. Methods Phys. A **559**(1), 143–147 (2006). doi:10.1016/j.nima.2005.11.207
26. D. del Re, Timing performance of the CMS ECAL and prospects for the future. J. Phys. Conf. Ser. **587**(1), 012003 (2015). doi:10.1088/1742-6596/587/1/012003
27. S. Abdullin, V. Abramov, B. Acharya et al., Design, performance, and calibration of CMS hadron-barrel calorimeter wedges. Eur. Phys. J. C **55**(1), 159–171 (2008). doi:10.1140/epjc/s10052-008-0573-y
28. S. Abdullin et al., Design, performance, and calibration of the CMS hadron-outer calorimeter. Eur. Phys. J. C **57**(3), 653–663 (2008). doi:10.1140/epjc/s10052-008-0756-6
29. G. Anzivino et al., Review of the hybrid photo diode tube (HPD) an advanced light detector for physics. Nucl. Instr. Methods Phys. A **365**(1), 76–82 (1995). doi:10.1016/0168-9002(95)00486-6
30. A. Lobanov, The CMS outer HCAL SiPM upgrade. J. Phys. Conf. Ser. **587**(1), 012005 (2015). doi:10.1088/1742-6596/587/1/012005
31. N. Akchurin, R. Wigmans, Hadron calorimetry. Nucl. Instr. Methods Phys. A **666**, 80–97 (2012). doi:10.1016/j.nima.2011.10.035
32. CMS Collaboration, CMS TriDAS project: Technical Design Report, Volume 1: The Trigger Systems, Technical Design Report CERN-LHCC-2000-038, CERN, Geneva (2002)
33. CMS Collaboration, CMS TriDAS Project: Technical Design Report, Volume 2: Data Acquisition and High-Level Trigger, Technical Design Report CERN-LHCC-2002-026, CERN, Geneva (2002)

34. CMS Collaboration, CMS High Level Trigger, Technical Report CERN-LHCC-2007-021, CERN, Geneva (2007)
35. CMS Collaboration, CMS Technical Design Report for the Level-1 Trigger Upgrade, Technical Report CERN-LHCC-2013-011. CMS-TDR-12, CERN, Geneva, Jun (2013)
36. CMS Collaboration, CMS Technical Design Report for the Phase 1 Upgrade of the Hadron Calorimeter, Technical Report CERN-LHCC-2012-015. CMS-TDR-10, CERN, Geneva, Sep (2012)
37. CMS Collaboration, Technical proposal for the upgrade of the CMS detector through 2020, Technical Report CERN-LHCC-2011-006, CERN, Geneva (2011)
38. CMS Collaboration, Technical Proposal for the Phase-II Upgrade of the CMS Detector, Technical Report CERN-LHCC-2015-010, CERN, Geneva. Geneva, Jun (2015)

http://www.springer.com/978-3-319-58879-7

CMS Pixel Detector Upgrade and Top Quark Pole Mass Determination
Spannagel, S.
2017, XXVII, 274 p. 136 illus., 74 illus. in color.,
Hardcover
ISBN: 978-3-319-58879-7